Momentum-space entanglement in Heisenberg spin-half ladders

Rex Lundgren

Phys. Rev. B **93**, 125107 — Published 2 March 2016

DOI: 10.1103/PhysRevB.93.125107

Momentum-Space Entanglement in Heisenberg Spin-Half Ladders

Rex Lundgren[1]

[1] *Department of Physics, The University of Texas at Austin, Austin, TX 78712, USA*

(Dated: February 3, 2016)

We study momentum-space entanglement in quantum spin-half ladders consisting of two coupled critical XXZ spin-half chains using field theoretical methods developed in Lundgren *et al.* [Phys. Rev. B **88**, 245137 (2013)], and exact diagonalization. When the system is gapped, we analytically find the momentum-space entanglement Hamiltonian is described by a chiral conformal field theory with a central charge of two. This is in contrast to entanglement Hamiltonians of various real-space partitions of gapped-spin ladders that have a central charge of one. When the system is gapless, the entanglement Hamiltonian consists of one gapless mode that is linear in subsystem momentum and one mode with a flat dispersion relation. In the gapless region, we extend the work of Lundgren *et al.* to include the effect of a certain irrelevant term on the entanglement spectrum. In both the gapless and gapped phases, the momentum-space entanglement entropy obeys a volume law. In the gapless region, we find a subleading constant term in the entanglement entropy which contains information about the underlying field theory of the system. The analytical predictions for the entanglement spectrum are consistent with results from exact diagonalization.

PACS numbers: 71.10.Pm, 03.67.Mn, 11.25.Hf

I. INTRODUCTION

Quantum entanglement has become an indispensable tool in the study of condensed matter physics. In particular, the topological entanglement entropy [1, 2] and the entanglement spectrum [3] have played a significant part in understanding and identifying exotic phases of matter. The entanglement spectrum is obtained as follows: First a system is partitioned into two regions, A and B. This partition is usually made in real-space. Given the reduced density matrix of A, ρ_A, where ρ_A is obtained from the full density matrix, ρ, (formed from the ground state wave-function) as $\rho_A = e^{-H_e} = \mathrm{Tr}_B(\rho)$, the entanglement spectrum is the set of eigenvalues of H_e, which is called the entanglement Hamiltonian. The entanglement entropy, S, can be obtained from the entanglement spectrum as $S = -\mathrm{Tr}\rho_A \ln \rho_A$. In a real-space partition, the entanglement entropy for topologically ordered states is equal to $\alpha|\partial A| - \gamma$, where α is a non-universal constant term, $|\partial A|$ is the length of the boundary between regions A and B, and γ is the topological entanglement entropy. The topological entanglement entropy and (real-space) entanglement spectra has been studied in many systems including quantum spin chains [4–14] and ladders [15–22], fractional quantum Hall systems [3, 23–33], Chern insulators [34, 35], symmetry broken phases [36, 37], topological insulators [38–42], and other systems in one [43, 44] and two dimensions [45–53].

Recently, several works on the entanglement entropy and spectrum in one dimension have used a momentum-space partition. This partition is motivated in part by the low-energy description of one-dimensional systems, which involves splitting particles into right and left movers [54, 55]. The momentum-space entanglement spectrum was first studied in the bosonic formulation of the Heisenberg spin-half chain [56], where it was found to reveal information about the underlying conformal field theory by the counting of entanglement levels and an entanglement gap. Ref. [57] studies the momentum-space entanglement spectrum of both fermionic and bosonic formulations of the XXZ spin-half chain. For the bosonic formulation, Ref. [57] finds that the entanglement gap seen in Ref. [56] does not extend throughout the critical region. For the fermionic formulation, the momentum-space entanglement Hamiltonian does not capture physical phase transitions. While this might seem like a drawback, Ref. [57] highlights that these results might be useful for numerical algorithms, such as the momentum-space density matrix renormalization group. The momentum-space entanglement spectrum has also proved useful in characterizing disordered fermionic systems [58, 59] and critical spin-1 chains [60]. Entanglement entropy between left and right movers was also recently studied in the context of string theory [61]. We note that the entanglement entropy of a momentum-space partition where fast modes were traced over, instead of partitioning left and right movers as done in this paper, was studied in Ref. [62].

Inspired by these results on the momentum-space entanglement spectrum, we analytically and numerically study the momentum-space entanglement spectrum and entropy between left and right movers in Heisenberg spin-half ladders. The legs of the ladder consist of spin-half XXZ chains of length L, described by the following Hamiltonian (with periodic boundary conditions):

$$H_\alpha = \sum_{i=1}^{L} \frac{J^{xy}}{2}(S^+_{\alpha,i}S^-_{\alpha,i+1} + S^-_{\alpha,i}S^+_{\alpha,i+1}) + J^z S^z_{\alpha,i}S^z_{\alpha,i+1}, \tag{1}$$

where $S^+_{\alpha,i}$, $S^-_{\alpha,i}$, and $S^z_{\alpha,i}$ are the standard spin-half operators on leg $\alpha \in \{1,2\}$ and site $i \in \{1,\ldots,L\}$. We take the interchain coupling between the legs of the ladder to

be

$$H_\perp = \sum_{i=1}^{L} \left(\frac{J_\perp^{xy}}{2}(S_{1,i}^+ S_{2,i}^- + S_{1,i}^- S_{2,i}^+) + J_\perp^z S_{1,i}^z S_{2,i}^z \right). \quad (2)$$

$H_\perp$ couples spins that are on the same rung of the ladder. The total Hamiltonian, which hosts both gapless and gapped phases, is then $H = H_1 + H_2 + H_\perp$. Throughout this work, we assume that $|J_\perp^{xy}|, |J_\perp^z| \ll J^{xy}$ and $J^{xy} > 0$.

By mapping the spin-ladder to a low-energy bosonic field theory and then expanding interchain interactions to quadratic order in fields (as done by Lundgren *et al.* [21]), we are able to analytically obtain the momentum-space entanglement spectrum and entropy between left and right movers. If the system is *gapped*, we notably find the entanglement spectrum is described by a chiral conformal field theory with a central charge of two. This is in contrast to the entanglement Hamiltonian with a central charge of one that has been found in various real-space partitions of gapped spin ladders (we note for these real-space partitions the entanglement Hamiltonian is non-chiral). These partitions include tracing out one leg of the ladder [15–17, 21, 22] and every other rung [63, 64]. If the system is *gapless*, the entanglement Hamiltonian has one gapless mode (with unit central charge one) and one dispersion-less mode. In the gapless region, we also include the effect of a certain formally irrelevant term (in the renormalization group sense) on the entanglement spectrum, extending the work of Ref. [21]. These analytical predictions are consistent with exact diagonalization results for system sizes up to 14 sites.

In addition, we find that the entanglement entropy scales with the length of the ladder, i.e. a volume law, regardless of whether the system is gapped or gapless. This volume law is also in contrast to the standard area law usually seen in real-space systems [65] (certain real-space systems can have volume laws [66–69]). We note that the entanglement entropy between coupled spin chains also scales with the length of the ladder (this is actually an example of the area law as the entanglement entropy between the coupled spin chains scale with the length of the partition) [70–72] . In the gapless case, we interestingly find a subleading constant term in the entanglement entropy that reveals information about the underlying field theory of the system.

Our paper is organized as follows: In Sec. II, we introduce the low-energy field theory of the spin ladder under study. In Sec. III, the momentum-space entanglement spectrum and entropy is calculated for this model. In Sec. IV, we compare our analytical predictions for the entanglement spectrum to exact diagonalization results. Finally, in Sec. V, we summarize our results and present our conclusion.

II. LOW-ENERGY FIELD THEORY

We now present the low-energy model of the system in terms of bosonic fields. See Ref. [54] or Ref. [55] for a review of Abelian bosonization. The transformation is summed up in the spin-to-boson transformation

$$S_\alpha^+(x) = \frac{S_{\alpha,i}^+}{\sqrt{a}} = \frac{e^{i\sqrt{\pi}\theta_\alpha(x)}}{\sqrt{2\pi a}}((-1)^{\frac{x}{a}} + \cos(\sqrt{4\pi}\phi_\alpha(x))) \quad (3)$$

and

$$S_\alpha^z(x) = \frac{S_{\alpha,i}^z}{a} = -\frac{1}{\sqrt{\pi}}\partial_x\phi_\alpha(x) + \frac{(-1)^{\frac{x}{a}}}{\pi a}\cos(\sqrt{4\pi}\phi_\alpha(x)), \quad (4)$$

where a is the lattice constant.

For this work, we consider the range of parameters for the legs of the ladder, $0 \leq \Delta = \frac{J^z}{J^{xy}} \leq 1$. For this range of Δ, the XXZ spin-half chain is critical and the bosonized Hamiltonian of a single chain takes the form

$$H_\alpha = \frac{u}{2}\int \mathrm{d}x \left(K(\partial_x\theta_\alpha)^2 + \frac{1}{K}(\partial_x\phi_\alpha)^2 \right), \quad (5)$$

where

$$K = \frac{\pi}{2(\pi - \cos^{-1}(\Delta))}, \; u = J^{xy}\frac{\pi\sqrt{1-\Delta^2}}{2\cos^{-1}(\Delta)}. \quad (6)$$

Each leg of the ladder is composed of left and right moving modes. At $K = 1$, there is no entanglement between left and right movers (when the legs of the ladder are uncoupled) [54, 55].

Introducing symmetric and anti-symmetric fields as follows

$$\phi_\pm = \frac{1}{\sqrt{2}}(\phi_1 \pm \phi_2), \; \theta_\pm = \frac{1}{\sqrt{2}}(\theta_1 \pm \theta_2), \quad (7)$$

the total Hamiltonian is

$$\begin{aligned} H = &\frac{u_+}{2}\int \mathrm{d}x \left(K_+(\partial_x\theta_+)^2 + \frac{1}{K_+}(\partial_x\phi_+)^2 \right) \\ &+ \frac{u_-}{2}\int \mathrm{d}x \left(K_-(\partial_x\theta_-)^2 + \frac{1}{K_-}(\partial_x\phi_-)^2 \right) + \\ &\frac{2G_a}{(2\pi a)^2}\int \mathrm{d}x \cos(\sqrt{2\pi}\theta_-) + \frac{2g_a}{(2\pi a)^2}\int \mathrm{d}x \cos(\sqrt{8\pi}\phi_-) + \\ &\frac{2g_s}{(2\pi a)^2}\int \mathrm{d}x \cos(\sqrt{8\pi}\phi_+) + \\ &\frac{1}{2}\frac{G_a}{(2\pi a)^2}\int \mathrm{d}x \cos(\sqrt{2\pi}\theta_-)\cos(\sqrt{8\pi}\phi_+), \end{aligned} \quad (8)$$

where $g_s = g_a = J_\perp^z a$, $G_a = \pi J_\perp^{xy} a$, and

$$K_\pm = K\left(1 \pm \frac{KJ_\perp^z a}{\pi u}\right)^{-\frac{1}{2}}, \; u_\pm = u\left(1 \pm \frac{KJ_\perp^z a}{\pi u}\right)^{\frac{1}{2}}. \quad (9)$$

We have ignored an umklapp term that is proportional to $J^z\cos(\sqrt{8\pi}\phi_+)\cos(\sqrt{8\pi}\phi_-)$ and another term proportional to $g_s\cos(\sqrt{2\pi}\theta_-)\cos(\sqrt{8\pi}\phi_-)$, as these two terms are always less relevant than the other terms for the range of parameters considered in this work. The

$\cos(\sqrt{2\pi}\theta_-)\cos(\sqrt{8\pi}\phi_+)$ term is less relevant than first three cosine terms and will not play an important role unless $J_\perp^z = 0$ (see Sec. II C).

For a wide range of Δ, Eq. (8) describes the Haldane phase for ferromagnetic rung coupling and the rung-singlet phase for anti-ferromagnetic rung coupling [54, 55, 73]. There are three cases of interest based on the relative scaling dimensions of the cosine terms. The scaling dimensions of $\cos(\sqrt{2\pi}\theta_-)$, $\cos(\sqrt{8\pi}\phi_-)$, $\cos(\sqrt{8\pi}\phi_+)$, are $(2K_-)^{-1}$, $2K_-$, $2K_+$ respectively. We now consider each of the three cases separately.

A. $J_\perp^{xy} \neq 0,\ J_\perp^z \neq 0,\ K_- \geq \frac{1}{2}$

We first consider the case when $J_\perp^z \neq 0$. For $J_\perp^z \neq 0$, the last term in Eq. (8) is less relevant than the other interaction terms and we ignore it. The symmetric and anti-symmetric modes are now separate. For $K_- \geq \frac{1}{2}$, the most relevant operator is the $\cos(\sqrt{2\pi}\theta_-)$ term [54], thus we drop the $\cos(\sqrt{8\pi}\phi_-)$ term (strictly speaking, at $K_- = \frac{1}{2}$, both cosine terms are equally relevant, but it is a useful approximation to neglect the $\cos(\sqrt{8\pi}\phi_-)$ term due to SU(2) symmetry present at $K_- = \frac{1}{2}$ [74].). The effective Hamiltonian for this range of parameters is then $H^A = H_+^A + H_-^A$, where

$$H_+^A = \frac{u_+}{2}\int \mathrm{d}x \left(K_+(\partial_x\theta_+)^2 + \frac{1}{K_+}(\partial_x\phi_+)^2\right) \frac{2g_s}{(2\pi a)^2}\int \mathrm{d}x \cos(\sqrt{8\pi}\phi_+) \quad (10)$$

and

$$H_-^A = \frac{u_-}{2}\int \mathrm{d}x \left(K_-(\partial_x\theta_-)^2 + \frac{1}{K_-}(\partial_x\phi_-)^2\right) + \frac{2G_a}{(2\pi a)^2}\int \mathrm{d}x \cos(\sqrt{2\pi}\theta_-). \quad (11)$$

For Δ between 0 and 1, both the symmetric and anti-symmetric channels are energetically gapped.

B. $J_\perp^z \neq 0,\ K_- < \frac{1}{2}$

We now consider the case when $K_- < \frac{1}{2}$. This set of parameters also includes the case when $J_\perp^{xy} = 0$, which is treated numerically later. The most relevant interaction term in the anti-symmetric channel is now the $\cos(\sqrt{8\pi}\phi_-)$ term [54], and we ignore the $\cos(\sqrt{2\pi}\theta_-)$ term. We note that, whereas, the symmetric channel is always gapped for the range of Δ considered, the anti-symmetric channel is gapless for a small region around $K = 1$ [73]. For example, if $J_\perp^z = .2$ the model is gapless from $\Delta = 0$ to $\Delta \approx .048$. More concretely, if $K_- < 1$ the anti-symmetric channel is gapped. The effective Hamiltonian for this range of parameters is $H^B = H_+^B + H_-^B$, where

$$H_+^B = \frac{u_+}{2}\int \mathrm{d}x \left(K_+(\partial_x\theta_+)^2 + \frac{1}{K_+}(\partial_x\phi_+)^2\right) \frac{2g_s}{(2\pi a)^2}\int \mathrm{d}x \cos(\sqrt{8\pi}\phi_+) \quad (12)$$

and

$$H_-^B = \frac{u_-}{2}\int \mathrm{d}x \left(K_-(\partial_x\theta_-)^2 + \frac{1}{K_-}(\partial_x\phi_-)^2\right) + + \frac{2g_a}{(2\pi a)^2}\int \mathrm{d}x \cos(\sqrt{8\pi}\phi_-). \quad (13)$$

C. $J_\perp^z = 0$

We finally consider the case when $J_\perp^z = 0$, which requires a bit more care, as less relevant operators become important. The Hamiltonian now reads,

$$H = \frac{u_+}{2}\int \mathrm{d}x \left(K_+(\partial_x\theta_+)^2 + \frac{1}{K_+}(\partial_x\phi_+)^2\right) + \frac{u_-}{2}\int \mathrm{d}x \left(K_-(\partial_x\theta_+)^2 + \frac{1}{K_-}(\partial_x\phi_+)^2\right) + \frac{2G_a}{(2\pi a)^2}\int \mathrm{d}x \cos(\sqrt{2\pi}\theta_-) + \frac{1}{2}\frac{G_a}{(2\pi a)^2}\int \mathrm{d}x \cos(\sqrt{2\pi}\theta_-)\cos(\sqrt{8\pi}\phi_+). \quad (14)$$

Under renormalization group flow, the $\cos(\sqrt{2\pi}\theta_-)$ term will increase, while the $\cos(\sqrt{2\pi}\theta_-)\cos(\sqrt{8\pi}\phi_+)$ term initially decreases [73]. As pointed out in Ref. [73], this means θ_- essentially becomes pinned and we can write the following effective Hamiltonian for the symmetric channel for this range of parameters as

$$H_+^C = \frac{u_+}{2}\int \mathrm{d}x \left(K_+(\partial_x\theta_+)^2 + \frac{1}{K_+}(\partial_x\phi_+)^2\right) + \frac{\lambda}{2}\frac{G_a}{(2\pi a)^2}\int \mathrm{d}x \cos(\sqrt{8\pi}\phi_+), \quad (15)$$

where $\lambda = \langle\cos(\sqrt{2\pi}\theta_-)\rangle$. The expectation value of $\cos(\sqrt{2\pi}\theta_-)$, λ, is taken with respect to

$$H_-^C = \frac{u_-}{2}\int \mathrm{d}x \left(K_-(\partial_x\theta_+)^2 + \frac{1}{K_-}(\partial_x\phi_+)^2\right) + \frac{2G_a}{(2\pi a)^2}\int \mathrm{d}x \cos(\sqrt{2\pi}\theta_-). \quad (16)$$

We thus see the effective Hamiltonians in Sec. II A and II C are the same upon swapping $J_\perp^z$ with $\lambda\pi J_\perp^{xy}/2$ in the symmetric channel. As such, we only need to calculate the entanglement spectrum for the Hamiltonian in Sec. II A and II B.

III. MOMENTUM-SPACE ENTANGLEMENT SPECTRUM AND ENTROPY

In this section, we calculate entanglement entropy and spectrum between left and right movers. These left and right movers are free only when the legs of the ladder are uncoupled and the legs of the ladder are at the XX point ($\Delta = 0$). This is equivalent to the momentum-space partition that is considered for the fermionic representation of the XXZ chain in Ref. [57].

We now calculate the entanglement Hamiltonian for the Hamiltonians in Secs. II A and II B. We first introduce left and right moving fields,

$$\phi_\alpha = \frac{\phi_{R,\alpha} + \phi_{L,\alpha}}{\sqrt{4\pi}},\ \theta_\alpha = \frac{\phi_{\alpha,L} - \phi_{\alpha,R}}{\sqrt{4\pi}}. \tag{17}$$

As mentioned earlier, when $K = 1$, the left and right movers of a single chain are free (when the legs of the ladder are not coupled). When $K \neq 1$ there is finite entanglement between left and right movers, even if the legs of the ladder are uncoupled, in this basis. The left and right moving fields have the following mode expansion [21]

$$\phi_{\alpha,R} = \phi_{\alpha,R,0} + 2\pi N_{\alpha,R}\frac{x}{L} + \sum_{k>0}\sqrt{\frac{2\pi}{L|k|}}\left(a^\dagger_{k,\alpha}e^{ikx} + a_{k,\alpha}e^{-ikx}\right) \tag{18}$$

and

$$\phi_{\alpha,L} = \phi_{\alpha,L,0} + 2\pi N_{\alpha,L}\frac{x}{L} + \sum_{k<0}\sqrt{\frac{2\pi}{L|k|}}\left(a^\dagger_{k,\alpha}e^{ikx} + a_{k,\alpha}e^{-ikx}\right). \tag{19}$$

Here, a_k are bosonic operators describing oscillator modes and $\phi_{\alpha,L/R,0}$ and $N_{\alpha,L/R}$ are the zero modes. The zero modes, $\phi_{\alpha,L/R,0}$ and $N_{\alpha,L,R}$, satisfy the commutation relations

$$[\phi_{\alpha,R,0}, N_{\alpha',R}] = -i\delta_{\alpha,\alpha'},\ [\phi_{\alpha,L,0}, N_{\alpha',L}] = i\delta_{\alpha,\alpha'}. \tag{20}$$

For completeness, the mode expansions of the symmetric and anti-symmetric fields, introduced in Eq. (7), are

$$\phi_\pm = \phi_{\pm,0} + \tilde{\pi}_\pm\frac{x}{L} + \sum_{k\neq 0}\sqrt{\frac{1}{2L|k|}}(a^\dagger_{k,\pm}e^{ikx} + a_{k,\pm}e^{-ikx}), \tag{21}$$

$$\theta_\pm = \theta_{\pm,0} + \pi_\pm\frac{x}{L} + \sum_{k\neq 0}\frac{\mathrm{sgn}(k)}{\sqrt{2L|k|}}(a^\dagger_{k,\pm}e^{ikx} + a_{k,\pm}e^{-ikx}), \tag{22}$$

where we have defined

$$\phi_{\pm,0} = \left(\frac{(\phi_{1,L,0} + \phi_{1,R,0}) \pm (\phi_{2,L,0} + \phi_{2,R,0})}{\sqrt{8\pi}}\right), \tag{23a}$$

$$\theta_{\pm,0} = \left(\frac{(\theta_{1,L,0} - \theta_{1,R,0}) \pm (\theta_{2,L,0} - \theta_{2,R,0})}{\sqrt{8\pi}}\right), \tag{23b}$$

$$\tilde{\pi}_{\pm,0} = \sqrt{\pi}\left(\frac{N_1 \pm N_2}{\sqrt{2}}\right), \tag{23c}$$

$$\pi_{\pm,0} = \sqrt{2\pi}\,(M_1 \pm M_2), \tag{23d}$$

$$a_{k,\pm} = \frac{(a_{k,1} \pm a_{k,2})}{\sqrt{2}}, \tag{23e}$$

where $N_\alpha = N_{1,L} + N_{1,R}$ and $M_\alpha = \frac{N_{1,L} - N_{1,R}}{2}$. In quantum spin chains, $N_\alpha, M_\alpha \in \mathbb{Z}$ [75]. The commutation relations (which can be derived using Eqs. (20) and (23)) that are important for this work are

$$[\phi_{+,0}, \pi_{+,0}] = i,\ [\theta_{-,0}, \tilde{\pi}_{-,0}] = i,\ [\phi_{-,0}, \pi_{-,0}] = i. \tag{24}$$

We now find the ground state of the total Hamiltonian, Eq. (8). After finding the ground state, we can easily obtain the momentum-space entanglement properties of the model. Following Ref. [21], we expand the cosine terms to quadratic order in field strength. In Ref. [21], the momentum-space entanglement spectrum and entropy was calculated for a single Tomonaga-Luttinger liquid. In the present case, we have two uncoupled Tomonaga-Luttinger liquids. However, we will see that analytical treatment of the zero modes is slightly different than for the case of a single Tomonaga-Luttinger liquid, so we provide a detailed derivation of the entanglement spectrum and entropy (the analytical treatment of the oscillator modes remains the same). The scalar fields from the quadratic Hamiltonian are then mode expanded and the Hamiltonian is diagonalized via a Bogoliubov transformation. For small values of $J_\perp$ and $J^z_\perp$, this expansion should be done after the coupling grows under renormalization group flow. As such, our approach is valid when the system size is larger than the correlation length. The analytical predictions obtained from this method have been numerically investigated with exact diagonalization in Ref. [21] and Ref. [57]. Excellent agreement was found between the analytical and numerical results. The method developed in Ref. [21] was also recently used to study the real-space entanglement spectrum of wire constructions of fractional quantum Hall phases [76].

While this approach works for a wide range of couplings, we note if the field is in a superposition of being localized on different minima of the cosine, this approach breaks down. However, due to the compactification of the bosonic fields in the Haldane and Rung-singlet phases, we do not have to worry about this issue in this work.

A. $J_\perp \neq 0,\ J^z_\perp \neq 0,\ K_- \leq \frac{1}{2}$

We first consider the Hamiltonian in Sec. II A. Recall these results also apply for the parameters in Sec. II C

upon switching $\lambda\pi J_\perp^{xy}/2$ for $J_\perp^z$ in the symmetric channel. We note that due to the locking of the ϕ_+ and θ_- fields, the winding modes of these fields must be suppressed, i.e. $\tilde{\pi}_+ = \pi_- = 0$. We expand the cosine terms as

$$\frac{2G_a}{(2\pi a)^2}\cos(\sqrt{2\pi}\theta_-) \approx \text{const.} + \frac{u_- m_{A,-}^2 K_-}{2}(\theta_- - \bar{\theta}_{-,0})^2 \tag{25}$$

and

$$\frac{2g_s}{(2\pi a)^2}\cos(\sqrt{8\pi}\phi_+) \approx \text{const.} + \frac{u_+ m_{A,+}^2}{2K_+}(\phi_+ - \bar{\phi}_{+,0})^2, \tag{26}$$

where $\bar{\phi}_{+,0}$ and $\bar{\theta}_{-,0}$ are the locking positions. Plugging in the mode expansion and writing $H_\pm = H_\pm^{\text{zero}} + H_\pm^{\text{osc}}$, we find for the oscillator portion,

$$H_\pm^{\text{osc}} = \frac{u_\pm}{2}\sum_{k\neq 0}\begin{pmatrix} a_{k,\pm}^\dagger, a_{-k,\pm}\end{pmatrix}\begin{pmatrix} A_{A,k,\pm} & B_{k,\pm} \\ B_{A,k,\pm} & A_{A,k,\pm}\end{pmatrix}\begin{pmatrix} a_{k,\pm} \\ a_{-k,\pm}^\dagger\end{pmatrix} \tag{27}$$

with

$$\begin{aligned} A_{A,k,+} &= \frac{1}{2}\left(\frac{1}{K_+} + K_+\right)|k| + \frac{m_{A,+}^2}{2|k|K_+}, \\ B_{A,k,+} &= \frac{1}{2}\left(\frac{1}{K_+} - K_+\right)|k| + \frac{m_{A,+}^2}{2|k|K_+}, \\ A_{A,k,-} &= \frac{1}{2}\left(\frac{1}{K_-} + K_-\right)|k| + \frac{K_- m_{A,-}^2}{2|k|}, \\ B_{A,k,-} &= \frac{1}{2}\left(\frac{1}{K_-} - K_-\right)|k| - \frac{K_- m_{A,-}^2}{2|k|}. \end{aligned} \tag{28}$$

By performing a Bogoliubov transformation,

$$\begin{pmatrix} a_{k,\pm} \\ a_{-k,\pm}^\dagger\end{pmatrix} = \begin{pmatrix} \cosh\theta_{k,\pm} & \sinh\theta_{k,\pm} \\ \sinh\theta_{k,\pm} & \cosh\theta_{k,\pm}\end{pmatrix}\begin{pmatrix} b_{k,\pm} \\ b_{-k,\pm}^\dagger\end{pmatrix}, \tag{29}$$

with

$$\begin{aligned} \cosh(2\theta_{A,k,\pm}) &= \frac{A_{A,k,\pm}}{\lambda_{A,k,\pm}}, \\ \sinh(2\theta_{A,k,\pm}) &= -\frac{B_{A,k,\pm}}{\lambda_{A,k,+}}, \\ \lambda_{A,k,\pm} &= \sqrt{A_{A,k,\pm}^2 - B_{A,k,\pm}^2} = \sqrt{k^2 + m_{A,\pm}^2}, \end{aligned} \tag{30}$$

the oscillator part of $H_\pm$ is diagonalized as

$$H_\pm = u_\pm \sum_{k\neq 0}\lambda_{A,k,\pm}\left(b_{k,\pm}^\dagger b_{k,\pm} + \frac{1}{2}\right). \tag{31}$$

We thus have a Klein-Gordon Hamiltonian with a mass gap $u_\pm m_{A,\pm}$. Renormalization group calculations to lowest order in $J_\perp$ and $J_\perp^z$ yields

$$m_{A,+} = \frac{u_+}{a}\left(\frac{4K_+ g_s}{\pi u_+}\right)^{\frac{1}{2-2K_+}} \tag{32}$$

and

$$m_{A,-} = \frac{u_-}{a}\left(\frac{4G_a}{\pi u_- K_-}\right)^{\frac{1}{2-\frac{2}{K_-}}}. \tag{33}$$

For the details of this calculation, see Ref. [54] or [55]. The ground state $|0\rangle$ of $H_\pm^A$ is specified by the condition that $b_{k,\pm}|0\rangle = 0$ for all $k \neq 0$. For the zero mode contribution we find

$$H_+^{\text{zero}} = \frac{u_+}{2}(\pi_+^2\frac{K_+}{L} + \frac{L m_{A,+}^2}{K_+}(\Delta\phi_{+,0})^2), \tag{34}$$

$$H_-^{\text{zero}} = \frac{u_-}{2}(\tilde{\pi}_-^2\frac{1}{LK_-} + L m_{A,-}^2 K_-(\Delta\theta_{-,0})^2), \tag{35}$$

where we have defined $\Delta\phi_{\pm,0} = \phi_{\pm,0} - \bar{\phi}_{\pm,0}$ and $\Delta\theta_{\pm,0} = \theta_{\pm,0} - \bar{\theta}_{\pm,0}$. We note that the reduced density matrix of left or right movers can be factored as $\rho_A = \rho_A^{\text{zero}} \otimes \rho_A^{\text{osc}}$. Furthermore, we can factorize ρ_A^{osc} as $\rho_{A,+}^{\text{osc}} \otimes \rho_{A,-}^{\text{osc}}$.

We are now in position to calculate the oscillator part of the reduced density matrix, ρ_A^{osc}, using methods of free theories originally introduced by Peschel [77]. We first calculate the two-point correlation function for right moving particles. This is given by

$$\langle 0|a_{k,\pm}^\dagger a_{k,\pm}|0\rangle = \sinh^2\theta_{k,\pm} = \frac{\cosh(2\theta_{k,\pm}) - 1}{2}. \tag{36}$$

Introducing the ansatz,

$$\rho_{A,\pm}^{\text{osc}} = \frac{1}{Z_{e,\pm}^{\text{osc}}}e^{-H_{e,\pm}^{\text{osc}}},\ Z_{e,\pm}^{\text{osc}} = \text{Tr}e^{-H_{e,\pm}^{\text{osc}}}, \tag{37}$$

with

$$H_{e,\pm}^{\text{osc}} = \sum_{k>0} w_{k,\pm}\left(a_{k,\pm}^\dagger a_{k,\pm} + \frac{1}{2}\right), \tag{38}$$

an alternate expression for the two-point correlation function is given by the Bose distribution function,

$$\text{Tr}(a_{k,\pm}^\dagger a_{k,\pm} e^{-H_{e,\pm}^{\text{osc}}}) = \frac{1}{e^{\omega_{k,\pm}} - 1}. \tag{39}$$

Here, $H_{e,\pm}^{\text{osc}}$ is the entanglement Hamiltonian for the right-moving oscillator modes. We stress the entanglement Hamiltonian is a different object than the physical Hamiltonian for the oscillator modes. Equating the two expressions for the two-point correlation function, we find

$$w_{k,\pm} = \ln\left(\frac{\cosh(2\theta_{k,\pm}) + 1}{\cosh(2\theta_{k,\pm}) - 1}\right). \tag{40}$$

Using Eq. (40), we find, to lowest order in sub-system momentum,

$$\begin{aligned} w_{A,+,k} &= v_{e,A,+}k = \frac{4K_+}{m_{A,+}}k, \\ w_{A,-,k} &= v_{e,A,-}k = \frac{4}{K_- m_{A,-}}k. \end{aligned} \tag{41}$$

The entanglement Hamiltonian for the symmetric (anti-symmetric resp.) oscillator part, is then

$$H_{e,A,\pm} = v_{e,A,\pm}\left(\sum_{k>0} k a^\dagger_{k,\pm} a_{k,\pm} - \frac{\pi}{12L}\right). \tag{42}$$

Here, we have used ζ-function regularization $\zeta(-1) = -\frac{1}{12}$ for the infinite constant term.

We now consider the zero-mode part of the entanglement spectrum. The commutation relations for the zero modes allow for the identification of the zero-mode Hamiltonian as a discrete harmonic oscillator. In the limit of large system size, the discreteness of the harmonic oscillator is irrelevant. As such, the ground-state in the $\pi_+, \tilde{\pi}_-$ basis can be approximated as a Gaussian,

$$\langle \pi_+, \tilde{\pi}_- | G\rangle \propto e^{-\frac{K_+(\pi_+)^2}{2m_{A,+}L} - \frac{(\tilde{\pi}_-)^2}{2m_{A,-}LK_-}}. \tag{43}$$

Using $\tilde{\pi}_+, \pi_- = 0$, the ground state can be written as

$$|G\rangle = \sum_{(\bar{M},\bar{N})} \frac{1}{\sqrt{z}} \exp\left[\frac{-\pi}{2L}\left(2v_{e,A,+}\bar{M}^2 + v_{e,A,-}\bar{N}^2\right)\right] \times |(M_1,N_1) = (\bar{M},\bar{N})\rangle \otimes |(M_2,N_2) = (\bar{M},-\bar{N})\rangle, \tag{44}$$

the reduced density matrix for right moving zero modes is then

$$\rho^{\text{zero}}_A = \sum_{N_{R,1},N_{R,2}} |N_{R,1},N_{R,2}\rangle e^{-\frac{2\pi K_+(N_{R,+})^2}{m_{A,+}L} - \frac{2\pi(N_{R,-})^2}{m_{A,-}LK_-}} \langle N_{R,1},N_{R,2}|. \tag{45}$$

where $N_{R,\pm} = N_{R,1} \pm N_{R,2}$. The total entanglement Hamiltonian for the zero-mode part is given by

$$H^{\text{zero}}_{e,A} = \frac{\pi}{2L}\left(v_{e,A,+}N^2_{R,+} + v_{e,A,-}N^2_{R,-}\right). \tag{46}$$

The total entanglement Hamiltonian for right moving particles is $H_{e,A} = H_{e,A,+} + H_{e,A,-} + H^{\text{zero}}_{e,A}$. Both $H_{e,A,-}$ and $H_{e,A,+}$ are gapless and have a chiral central charge of one, thus $H_{e,A}$ is gapless and has a chiral central charge of two.

We now calculate the entanglement entropy, S, in the large L limit. Following the method first outlined in Ref. [21], we calculate the partition function (at a fictious temperature, $T = \frac{1}{\beta}$) which is given by

$$Z_{e,A}(\beta) = Z^{\text{zero}}_{e,A}(\beta) Z^{\text{osc}}_{e,A,-}(\beta) Z^{\text{osc}}_{e,A,+}(\beta). \tag{47}$$

The partition function for the oscillators is

$$Z^{\text{osc}}_{e,A,\pm}(\beta) = e^{\frac{\pi}{12}\tau_{2,\pm}} \prod_{j=1}^{\infty}\left(\frac{1}{1-e^{-2\pi\tau_{2,A,\pm}j}}\right) = \frac{1}{\eta(i\tau_{2,\pm})}, \tag{48}$$

where η is the Dedekind eta function and $\tau_{2,A,\pm} = \frac{\beta v_{e,A,\pm}}{L}$. As $L\to\infty$, we have

$$Z^{\text{osc}}_{e,A,\pm}(\beta) \approx e^{\frac{LT\pi}{v_{e,A,\pm}12}}\sqrt{\frac{v_{e,A,\pm}}{LT}}. \tag{49}$$

The partition function for the symmetric zero-mode channel is

$$Z^{\text{zero}}_{e,A} = \sum_{N_{1,R},N_{2,R}} e^{-\frac{\beta\pi}{2LK}(\mathbf{N}^T_R\Omega\mathbf{N}_R)} = \sum_{N_{1,R},N_{2,R}} e^{-\pi\tau(\mathbf{N}^T_R\Omega\mathbf{N}_R)}, \tag{50}$$

where

$$\Omega = \begin{pmatrix} v_{e,A,+}+v_{e,A,-} & v_{e,A,+}-v_{e,A,-} \\ v_{e,A,+}-v_{e,A,-} & v_{e,A,+}+v_{e,A,-}\end{pmatrix}, \tag{51}$$

$\mathbf{N}_R = \begin{pmatrix} N_{1,R}, & N_{2,R}\end{pmatrix}$, and $\tau = \frac{\beta}{2L}$. The partition function for zero modes is the Riemann theta function. Using the modular properties of the Riemann theta function, in the large L limit we find

$$Z^{\text{zero}}_{e,A} = \frac{\theta(0|i\tau^{-1}\Omega^{-1})}{\sqrt{\det(\tau\Omega)}} \approx \left(\frac{v_{e,A,+}v_{e,A,-}\beta^2}{L^2K^2}\right)^{-\frac{1}{2}}. \tag{52}$$

Here, we have used the fact that the Riemann theta function approaches unity as L goes to infinity. The total partition function is then

$$Z_{e,A} = e^{\frac{LT\pi}{12}\left(\frac{1}{v_{e,A,+}}+\frac{1}{v_{e,A,-}}\right)} \tag{53}$$

The momentum-space entanglement entropy for this partition is then

$$S = \frac{\partial(T\ln Z_{e,A})}{\partial T}|_{T=1} = L\frac{\pi}{6}\left(\frac{v_{e,A,+}+v_{e,A,-}}{v_{e,A,+}v_{e,A,-}}\right). \tag{54}$$

We thus see we have a volume law. The physical reason for the volume law is quite clear. We see that from Eq. (27), there is pairing between states with momentum k and momentum $-k$. In other words, the Hamiltonian generates entanglement between pairs of left and right moving particles with momentum k. The number of these pairs is proportional to the number of momentum modes. The number of momentum modes is directly proportional to the system size, hence giving rise to a volume law for the momentum-space entanglement entropy.

B. $J^z_\perp \neq 0,\ K_- > \frac{1}{2}$

1. *Gapped Regime*

We now consider the Hamiltonian in Sec. II B. If the anti-symmetric channel is gapped, we expand that cosine term in the anti-symmetric channel as

$$\frac{2g_a}{(2\pi a)^2}\cos(\sqrt{8\pi}\phi_-) \approx \text{const.} + \frac{u_-m^2_{B,-}}{2K_-}(\phi_- - \bar{\phi}_{-,0})^2. \tag{55}$$

Due to the locking of the ϕ_+ and ϕ_- fields, we have $\tilde{\pi}_- = \tilde{\pi}_+ = 0$. After plugging in the mode expansions, we find for the oscillator contribution

$$H_{\pm}^{\rm osc} = \frac{u_{\pm}}{2}\sum_{k\neq 0}\begin{pmatrix} a^{\dagger}_{k,\pm}, a_{-k,\pm}\end{pmatrix}\begin{pmatrix} A_{B,k,\pm} & B_{B,k,\pm} \\ B_{B,k,\pm} & A_{B,k,\pm}\end{pmatrix}\begin{pmatrix} a_{k,\pm} \\ a^{\dagger}_{-k,\pm}\end{pmatrix}, \tag{56}$$

with

$$\begin{aligned} A_{B,k,+} &= \frac{1}{2}\left(\frac{1}{K_+} + K_+\right)|k| + \frac{m_{B,+}^2}{2|k|K_+}, \\ B_{B,k,+} &= \frac{1}{2}\left(\frac{1}{K_+} - K_+\right)|k| + \frac{m_{B,+}^2}{2|k|K_+}, \\ A_{B,k,-} &= \frac{1}{2}\left(\frac{1}{K_-} + K_-\right)|k| + \frac{m_{B,-}^2}{2|k|K_-}, \\ B_{B,k,-} &= \frac{1}{2}\left(\frac{1}{K_-} - K_-\right)|k| - \frac{m_{B,-}^2}{2|k|K_-}. \end{aligned} \tag{57}$$

We again have a sine-Gordon model with a mass gap, $u_{\pm}m_{B,\pm}$. Renormalization group calculations to lowest order in $J_\perp$ and $J_\perp^z$ yield

$$m_{B,+} = \frac{u_+}{a}\left(\frac{4K_+ g_s}{\pi u_+}\right)^{\frac{1}{2-2K_+}} \tag{58}$$

and

$$m_{B,-} = \frac{u_-}{a}\left(\frac{4K_- g_a}{\pi u_-}\right)^{\frac{1}{2-2K_-}}. \tag{59}$$

We find the zero-mode contribution to be

$$H_+^{\rm zero} = \frac{u_+}{2}(\pi_+^2\frac{K_+}{L} + \frac{Lm_{B,+}^2}{K_+}(\Delta\phi_{+,0})^2), \tag{60}$$

$$H_-^{\rm zero} = \frac{u_-}{2}(\pi_-^2\frac{K_-}{L} + \frac{Lm_{B,-}^2}{K_-}(\Delta\phi_{-,0})^2). \tag{61}$$

Following similar steps as the previous section, we find the entanglement Hamiltonian for the oscillators to be

$$H_{e,B,\pm}^{\rm osc} = v_{e,B,\pm}\left(\sum_{k>0} k a^{\dagger}_{k,\pm}a_{k,\pm} - \frac{\pi}{12L}\right), \tag{62}$$

where

$$v_{e,B,+} = \frac{4K_+}{m_{B,+}},\ v_{e,B,-} = \frac{4}{K_- m_{B,-}}. \tag{63}$$

Using $\tilde{\pi}_+, \tilde{\pi}_- = 0$, we find the zero-mode contribution of the entanglement Hamiltonian to be

$$H_{e,B}^{\rm zero} = \frac{\pi}{2L}\left(v_{e,B,+}N_{R,+}^2 + v_{e,B,-}N_{R,-}^2\right). \tag{64}$$

Evaluating the partition function in the same manner as the previous section, we find the entanglement entropy to be

$$S = L\frac{\pi}{6}\left(\frac{v_{e,B,+}+v_{e,B,-}}{v_{e,B,+}v_{e,B,-}}\right). \tag{65}$$

2. *Gapless Regime*

We can also treat the small gapless region of the anti-symmetric channel at $J_\perp^{xy} = 0$ and $K_- > 1$. One can show in this case (by neglecting the irrelevant cosine term. Strictly speaking, the irrelevant cosine terms will modify these results as discussed in detail below. We will see the main effect of the irrelevant cosine terms can be accounted for by replacing the Tomonaga-Luttinger parameter, K_-, with an effective one.) the entanglement spectrum for the anti-symmetric mode is flat and $w_{B,-,k}$ is given by [21]

$$w_{B,-,k} = w_{B,-} = \ln\left(\frac{K_- + (K_-)^{-1} + 2}{K_- + (K_-)^{-1} - 2}\right). \tag{66}$$

The entanglement Hamiltonian for the anti-symmetric oscillator modes is then

$$H_{e,B,-}^{\rm osc} = w_{B,-}\left(\sum_{k>0} a^{\dagger}_{k,\pm}a_{k,\pm} + \frac{1}{2}\right). \tag{67}$$

The entanglement Hamiltonian for the symmetric oscillator modes is still given by Eq. (62). The zero mode entanglement Hamiltonian is given by

$$H_{e,B}^{\rm zero} = \frac{\pi v_{B,+}}{L}\bar{N}_+^2 \tag{68}$$

where $\bar{N}_+ \in \{-\infty, \ldots, \infty\}$. We see the symmetric part of the entanglement Hamiltonian remains gapless, and we thus have an entanglement Hamiltonian with one gapless mode and one dispersion-less, i.e. flat, mode.

After obtaining the entanglement Hamiltonian, one can calculate the momentum-space entanglement entropy. The entanglement entropy (See App. A for key steps of this calculations) is given by

$$S = L\left(\frac{\gamma}{2} + \frac{\pi}{6v_{e,B,+}}\right) - \kappa, \tag{69}$$

where

$$\kappa = \frac{(K_- - 1)^2}{4}\left[1 - \ln\left(\frac{(K_- - 1)^2}{4}\right)\right]. \tag{70}$$

In addition to the volume law, we have a subleading constant term in the entanglement entropy. This constant term reveals the Tomonaga-Luttinger parameter of the anti-symmetric gapless mode (once taking into account the irrelevant cosine term, we will see that κ actually reveals the effective Tomonaga-Luttinger parameter). We remark that the constant term that appears in the entanglement entropy between coupled Tomonaga-Luttinger liquids contains information on both the symmetric and anti-symmetric channels [70].

In general, there will be corrections to $w_{B,-}$ and the entanglement entropy due to the irrelevant cosine term we neglected in Eq. (13) (we are ignoring the three neglected terms that are less relevant). Finding these corrections

is crucial for obtaining qualitative agreement with some of the numerical results presented in the next section. We can treat the irrelevant cosine term in Eq. (13) as follows. The correlation functions in the gapless region can be computed from a perturbative expansion of the cosine term for small coupling strengths. Here, we focus on the correlation function of the exponential of the ϕ_- field. When $g_a = 0$, the correlation function is given by

$$\langle e^{ia\sqrt{2\pi}\phi_-(r)} e^{-ia\sqrt{2\pi}\phi_-(0)}\rangle = \left(\frac{a}{r}\right)^{a^2 K_-}, \tag{71}$$

where $r \gg a$. To second order in coupling strength, g_a, the correlation functions are given by (see for example, Ref. [54])

$$\langle e^{ia\sqrt{2\pi}\phi_-(r)} e^{-ia\sqrt{2\pi}\phi_-(0)}\rangle = \left(\frac{a}{r}\right)^{a^2 K_-^{eff}}, \tag{72}$$

where

$$K_-^{eff} = K_- - \frac{g_a^2}{2\pi^2 u_-^2}\int_a^L \frac{dr}{a}\left(\frac{r}{a}\right)^{3-4K_-} = K_- + \frac{g_a^2}{2\pi^2 u_-^2}\left(1 - \left(\frac{L}{a}\right)^{4-4K_-}\right)\frac{1}{4-4K_-}. \tag{73}$$

Here, L acts as an infrared cut-off. Since the exponent of correlation functions control the low-energy properties of the Hamiltonian [54], we can replace K_- by K_-^{eff} in gapless region and use the following effective Hamiltonian to describe the gapless region around $g_a = 0$

$$H_-^{B,eff} = \frac{u_-}{2}\int \mathrm{d}x \left(K_-^{eff}(\partial_x\theta_-)^2 + \frac{1}{K_-^{eff}}(\partial_x\phi_-)^2\right). \tag{74}$$

We also see that K_-^{eff} is smaller than K_-. Intuitively this makes sense because the cosine term acts to order ϕ_-, thereby making fluctuations less likely. The momentum-space entanglement spectrum and entropy (including κ) are still given by Eq. (66) and Eq. (69) respectively, except with K_-^{eff} replacing K_-.

IV. NUMERICAL ANALYSIS

In this section, we compare our predictions with exact diagonalization results for up to systems sizes of 14 sites (28 total spins). One can either transform the spin operators to Jordan-Wigner fermions or hard-core bosons. Using hard-core bosons is complicated by the fact that the commutation relation of hard-core boson creation and annihilation operators depend on the occupancy of a given state and thus the calculation of matrix elements between momentum basis states is numerically challenging. Thus, we consider a Jordan-Wigner transformation of the spin operators to spin-less fermions. In general, a Jordan-Wigner transformation will have long-range interactions and complicated boundary terms due to string factors. We will see that when $J_\perp^{xy} = 0$, the problem simplifies and we are able to obtain results consistent with the analytical predictions for the Hamiltonian in Sec. II B. Unfortunately, due to complicated boundary terms introduced by the Jordan-Wigner string we can not capture the results of Sec. II A and II C with a Jordan-Wigner transformation. We leave numerical verification of the analytical predictions of Sec. II A and II C for future work.

We begin by applying a Jordan-Wigner transformation to Eqs. (1) and (2). The Jordan-Wigner transformation is applied directly, i.e. all spins are arranged in a one dimensional sequence [78]. Explicitly, the Jordan-Wigner transformation is given by $S_i^- = c_i e^{i\pi\sum_{j<i} c_j^\dagger c_j}$, $S_i^z = (c_j^\dagger c_j - \frac{1}{2})$, where $i \in \{1,\ldots,2L\}$. We stress that one can not apply the Jordan-Wigner transformation separately to each leg of the ladder as this does not preserve the original algebra of the spin operators. The Hamiltonian for the legs of the ladder when written as a one-dimensional sequence of $2L$ spins is

$$\begin{aligned} H_1 + H_2 = &\sum_{i=1}^{L-1}\frac{J^{xy}}{2}(S_i^+S_{i+1}^- + S_i^-S_{i+1}^+) + J^z S_i^z S_{i+1}^z + \\ &\sum_{i=L+1}^{2L-1}\frac{J^{xy}}{2}(S_i^+S_{i+1}^- + S_i^-S_{i+1}^+) + J^z S_i^z S_{i+1}^z + \\ &\frac{J^{xy}}{2}(S_1^+S_L^- + S_1^-S_L^+) + J^z S_1^z S_L^z + \\ &\frac{J^{xy}}{2}(S_{L+1}^+S_{2L}^- + S_{L+1}^-S_{2L}^+) + J^z S_{L+1}^z S_{2L}^z. \end{aligned} \tag{75}$$

The last four terms in Eq. (75) arise due to periodic boundary conditions. The interchain coupling is

$$H_\perp = \sum_{i=1}^{L}\left(\frac{J_\perp^{xy}}{2}(S_i^+S_{i+L}^- + S_i^-S_{i+L}^+) + J_\perp^z S_i^z S_{i+L}^z\right). \tag{76}$$

Defining $\alpha_i = c_i \;\forall\; i < L+1, \quad \beta_i = c_i \;\forall\; i > L$, the Hamiltonian for the legs of the ladder (neglecting constant terms) is given by (for $J_\perp^{xy} = 0$)

$$H = \sum_{i=1}^{L}\left[\frac{J^{xy}}{2}(\alpha_i^\dagger\alpha_{i+1} + \alpha_{i+1}^\dagger\alpha_i + \beta_i^\dagger\beta_{i+1} + \beta_{i+1}^\dagger\beta_i) + J^z(\alpha_i^\dagger\alpha_i\alpha_{i+1}^\dagger\alpha_{i+1} + \beta_i^\dagger\beta_i\beta_{i+1}^\dagger\beta_{i+1}) + J_\perp^z\alpha_i^\dagger\alpha_i\beta_i^\dagger\beta_i\right]. \tag{77}$$

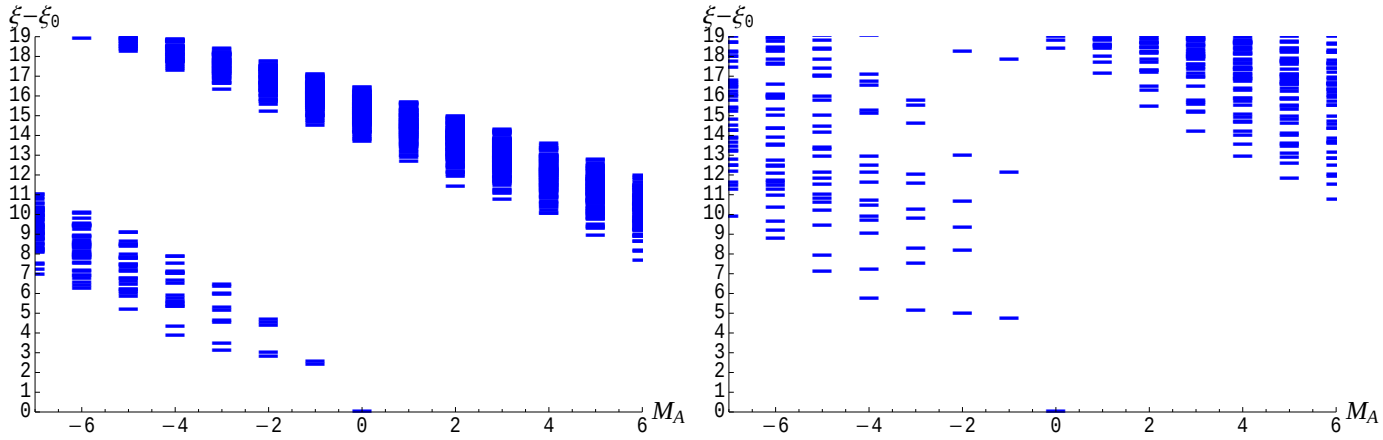

(a) $J^{xy}=1,\ J^{z}=1,\ J^{z}_{\perp}=.4,\ J^{xy}_{\perp}=0$ (b) $J^{xy}=1,\ J^{z}=.1,\ J^{z}_{\perp}=.6,\ J^{xy}_{\perp}=0$

FIG. 1. (color online) Fermionic entanglement spectra for representative values of Δ, with $L=14$ and $N_A=8$ (four particles on each leg). The entanglement eigenvalues, ξ, (relative to ξ_0, which is the ground state entanglement energy) are plotted versus the subsystem crystal momentum, M_A (we have also shifted the crystal momentum to have the lowest level at zero). (a) The low energy properties of the entanglement Hamiltonian are consistent with a chiral CFT with a central charge of two. (b) At $M_A=1$, we observe a large splitting of the first two entanglement levels, consistent with the prediction of a dispersion-less mode and a chiral conformal field theory of unit central charge.

We now introduce the Fourier transform of the creation and annihilation operators,

$$\alpha_i=\sum_{m=1}^{L}e^{i\frac{2\pi}{L}m}\tilde{\alpha}_m,\quad \beta_i=\sum_{k=1}^{L}e^{i\frac{2\pi}{L}k}\tilde{\beta}_k. \tag{78}$$

Here, $m\in\{1,\dots,L\}$ is the crystal momentum of the α-particles and $k\in\{1,\dots,L\}$ is the crystal momentum of the β-particles. The ground state of Eq. (75) has $\sum_{i=1}^{L}S^z_i=0$ and $\sum_{i=L+1}^{2L}S^z_i=0$. As such, we have $\frac{L}{2}$ α-particles and $\frac{L}{2}$ β-particles. To avoid a degenerate Fermi sea at $K=1$ (and when the legs of the ladder are uncoupled), we limit ourselves to systems sizes of $L=4n+2$, $n\in\mathbb{N}$.

After numerically finding the ground state in the momentum-space occupation basis, one can then find the momentum-space entanglement spectrum. The system is partitioned into two regions A and B in momentum-space. These regions are defined as $A=\{m|m\leq\frac{L}{2}\}\otimes\{k|k\leq\frac{L}{2}\}$ and $B=\{k|k>\frac{L}{2}\}\otimes\{m|m>\frac{L}{2}\}$. Regions A and B are decomposed in terms of the total crystal momentum, $M=M_A+M_B$ and total number of particles, $N=N_A+N_B$. N_A, N_B, M_A and M_B are given by

$$\begin{aligned}
M_A&=\Big(\sum_{m=1}^{\frac{L}{2}}n_{\alpha,m}m+\sum_{k=1}^{\frac{L}{2}}n_{\beta,k}k\Big)\bmod L,\\
M_B&=\Big(\sum_{m=\frac{L}{2}+1}^{L}n_{\alpha,m}m+\sum_{k=\frac{L}{2}+1}^{L}n_{\beta,k}k\Big)\bmod L,\\
N_A&=\sum_{m=1}^{\frac{L}{2}}n_{\alpha,m}+\sum_{k=1}^{\frac{L}{2}}n_{\beta,k},\\
N_B&=\sum_{m=\frac{L}{2}+1}^{L}n_{\alpha,m}+\sum_{k=\frac{L}{2}+1}^{L}n_{\beta,k}.
\end{aligned} \tag{79}$$

We now present our numerical results for the momentum-space entanglement spectrum of spin ladders.

A. Gapped Region

We first investigate the momentum-space entanglement spectrum of the gapped phase. We take $L=14$ (the largest system size available) and $N_A=8$ (four α particles and four β particles). Fig. 1a shows the entanglement spectrum at $J^{\perp}_z=.4$, $J^{xy}=1$, $J^z=1$. Starting from $M_A=0$, we observe a nearly linear spectrum with the following counting of entanglement levels $1,2,5,10,\dots$ (from right to left). This matches the counting of a chiral conformal field theory with a central charge of two, consistent with our analytical predictions.

From computing correlation functions, we find the correlation length for the Hamiltonian in Sec. II B is rather

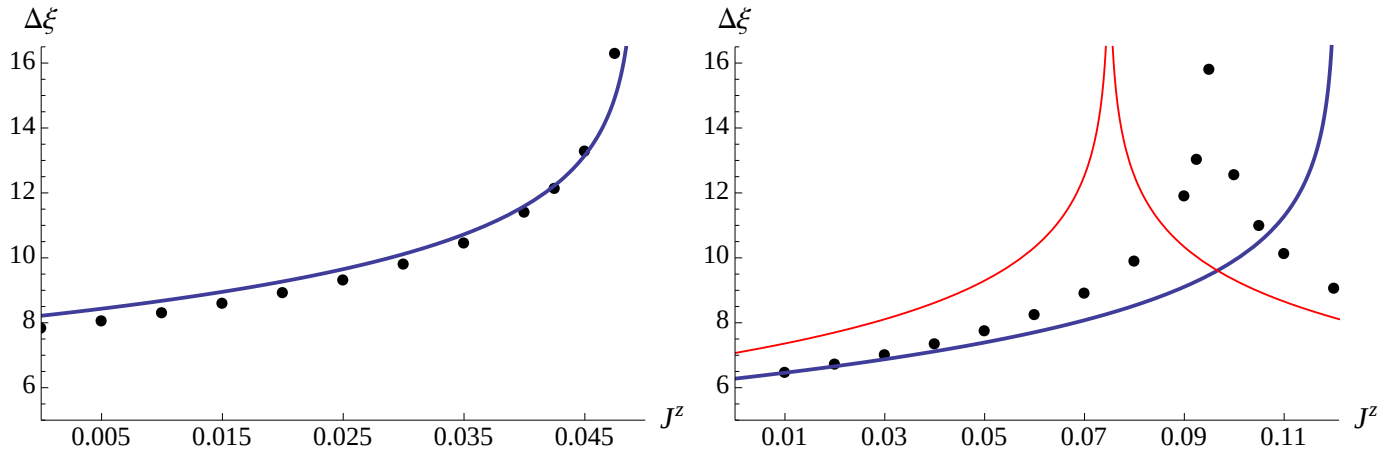

(a) $J^{xy} = 1,\ J^z_\perp = .2,\ J^{xy}_\perp = 0$ (b) $J^{xy} = 1,\ J^z_\perp = .5,\ J^{xy}_\perp = 0$

FIG. 2. (color online) The entanglement gap, $\Delta\xi$, between ξ_2 and ξ_0 versus J^z, with $L = 10$ and $N_A = 3$ (three particles on each leg). The black dots are numerical data obtained from exact diagonalization, the blue line is the analytical prediction using K_-, and the red line is the analytical prediction using K_-^{eff}.

large and on the same order of the system sizes considered in this work. The correlation length of the symmetric channel, $\xi_s \approx \frac{1}{m_{B,+}}$, is actually much larger than the correlation length in commonly studied isotropic Heisenberg ladders [79]. For the system sizes considered, this makes accurately verifying our analytical predictions for the slope of the entanglement spectrum difficult. Furthermore, there is a large computational cost to obtain the entanglement spectrum for each parameter point for the largest system size presented (14 sites). We thus leave a detailed numerical investigation of the slope of the momentum-space entanglement spectrum in spin-half ladders as an open problem.

B. Gapless Region

We now turn to the entanglement spectrum in the gapless region, where one expects to see one gapless mode and one flat mode. Shown in Fig. 1b is the entanglement spectrum at $J^{xy} = 1,\ J^z = .1,\ J^z_\perp = .6,\ J^{xy}_\perp = 0$. We observe at $M_A = 1$ a large splitting of the first two entanglement levels, consistent with the prediction of a chiral conformal field theory of unit central charge and a flat mode. In addition, the value of the second entanglement level at $M_A = 1$, which we call ξ_2, (12.06) is consistent with our analytical predictions (9.73) (using the effective Luttinger parameter, Eq. (73)). We expect the disagreement between the value of ξ_2 obtained numerically and our analytical prediction can be explained by a combination of higher order corrections of K_-^{eff} and taking into the other three irrelevant terms (which are less relevant than the cosine term in Eq. (13)). We are unable to use the entanglement levels at $M_A = 2$ to verify our analytical predictions due to their almost equal spacing. Larger systems sizes should allow one distinguish the entanglement levels that belong to the chiral conformal field theory and the flat mode at $M_A > 1$.

None the less, we can take a closer look at ξ_2 for various parameters to verify our analytical predictions. For $L = 10$ and $N_A = 6$ (three particles on each leg), we first investigate ξ_2 for $J^{xy} = 1,\ J^z_\perp = .2,\ J^{xy}_\perp = 0$ as a function of J^z. For $J^z_\perp = .2$, we are in the gapless region for $J^z = 0$ to $J^z \approx .048$. We see that our analytical prediction is in excellent agreement with our numerical results (see Fig. 2a). Note, this $J^z_\perp$ is much smaller than the one used in Fig. 1b, so higher order corrections to K_- are not important and thus we have better agreement between numerics and our analytical prediction. We note for this small value of $J^z_\perp$, K_-^{eff} and K_- are in near agreement. We now investigate ξ_2 for $J^z_\perp = .5$, which is shown in Fig. 2b. For $J^z_\perp = .5$, we are in the gapless region for $J^z = 0$ to $J^z \approx .12$. Notably, we see that analytical prediction for ξ_2 using K_-^{eff} and K_- are qualitatively *different*. More specifically, ξ_2 computed with K_-^{eff} diverges before the cosine term becomes relevant, while ξ_2 computed with K_- diverges exactly when the cosine term becomes relevant. We see that K_-^{eff} qualitatively captures the numerically observed behavior. Again, we expect better quantitative agreement if one where to include higher order corrections K_-^{eff} and use larger system sizes.

Finally, we remark that, while it would be interesting to numerically capture the predicted constant term in the entanglement entropy, it would be hard due to the finite size effects present for the system sizes considered in this section. More specifically, in deriving the entanglement entropy in the gapless phase, we neglected corrections to the entanglement entropy from sub-leading terms (in system size) in the symmetric channel.

V. CONCLUSION

We have studied the momentum-space entanglement entropy and spectrum of anisotropic spin-half ladders using field theoretical methods and exact diagonalization. We found that the entanglement entropy between left and right movers is linear in system size and obeys a volume law. When the system is gapped, the momentum-space entanglement Hamiltonian was found to be gapless and described by a chiral conformal field theory with a central charge of two. If the system is gapless, the entanglement Hamiltonian was found to be described by one chiral dispersion-less mode and one chiral gapless mode with a linear spectrum. We have extended the work of Ref. [21] by taking into account certain irrelevant terms, which qualitatively change the entanglement spectrum. In both the gapless and gapped regions, we find a volume law. Notably, in the gapless region we also find a subleading constant term. Exact diagonalization results are found to be consistent with our analytical predictions. Our work can easily be generalized to include exchange between the spins across diagonals of the plaquettes and the following four-spin term $(S_{1,i}S_{1,i+1}S_{2,i}S_{2,i+1})$, which can arise due to phonons.

As mentioned throughout this work, exact diagonalization suffers from finite size effects, as the typical correlation length of the phases studied in this work is on the same order as the system sizes currently available via exact diagonalization. As such, it would be interesting to numerically investigate the entanglement spectrum via quantum monte carlo methods, which have recently been applied to entanglement spectra studies [80–83], or the momentum-space density matrix renormalization group. Finally, it would also be interesting to generalize our work to study other gapless phases of spin ladders, including the vector chiral phase [84], and inequivalent chains.

ACKNOWLEDGMENTS

We thank R. Thomale, M. Oshikawa, K. Rasmussen, and R. Santos for useful exchanges and J. Blair for helpful discussions on exact diagonalization. We also thank S. Furukawa, P. Laurell, and G. Fiete for a critical reading of the manuscript, many helpful discussions, and collaboration on related work. R.L. was supported by National Science Foundation (NSF) Graduate Research Fellowship award number 2012115499 and NSF Grant No. DMR-0955778.

Appendix A: Momentum-Space Entanglement Entropy in Gapless Region

In this section, we provided some key steps in the calculation of the momentum-space entanglement entropy for the Hamiltonian in Sec. II B. The partition function for the anti-symmetric oscillator mode is given by

$$Z^{\rm osc}_{e,-}(\beta)=\prod_{k>0}\left(2\sin(\frac{\beta w_{k,B,-}}{2})\right)^{-1}=\left(2\sin(\frac{\beta w_{B,-}}{2})\right)^{-\frac{L}{2a}-1}. \tag{A1}$$

Here, we have used the fact that k runs over $\frac{L}{2a}-1$ modes (after taking into account the exclusion of the zero mode). We first calculate the Renyi entropy (for general Renyi index, n), which is given by

$$S_n=-\frac{1}{n-1}\ln\left(\frac{Z^{\rm osc}_{e,-}(n)}{Z^{\rm osc}_{e,-}(1)^n}\right)=\left(\frac{L}{2a}-1\right)\frac{1}{n-1}\ln\left(\frac{2\sinh(\frac{nw_{B,-}}{2})}{(2\sinh(\frac{w_{B,-}}{2}))^n}\right)=\left(\frac{L}{2a}-1\right)\frac{1}{n-1}\ln\left(\frac{1-e^{-nw_{B,-}}}{(1-e^{-w_{B,-}})^n}\right). \tag{A2}$$

After some algebra, we have

$$S_n=\left(\frac{L}{2a}-1\right)\frac{1}{n-1}\ln\left(\frac{1-(\frac{K_--1}{K_-+1})^{2n}}{(1-(\frac{K_--1}{K_-+1})^2)^n}\right)=\left(\frac{L}{2a}-1\right)\frac{1}{n-1}\left[\ln\left(1-(\frac{K_--1}{K_-+1})^{2n}\right)-n\ln\left(1-(\frac{K_--1}{K_-+1})^2\right)\right. \tag{A3}$$

For the parameters we are interested in, $K_-\approx 1$. For $K_-\approx 1$, we have

$$\ln\left(1-(\frac{K_--1}{K_-+1})^{2n}\right)\approx-\left(\frac{K_--1}{2}\right)^{2n}. \tag{A4}$$

Finally, we arrive at our expression for the Renyi entropy,

$$S_n=\left(\frac{L}{2a}-1\right)\frac{1}{n-1}\left[-\left(\frac{K_--1}{2}\right)^{2n}+n\left(\frac{K_--1}{2}\right)^2\right]. \tag{A5}$$

Taking the $n=1$ limit to obtain the entanglement entropy, we find

$$S_1=\left(\frac{L}{2a}-1\right)\frac{(K_--1)^2}{4}\left[1-\ln\left(\frac{(K_--1)^2}{4}\right)\right]. \tag{A6}$$

[1] M. Levin and X.-G. Wen, Phys. Rev. Lett. **96**, 110405 (2006).
[2] A. Kitaev and J. Preskill, Phys. Rev. Lett. **96**, 110404 (2006).
[3] H. Li and F. D. M. Haldane, Phys. Rev. Lett. **101**, 010504 (2008).
[4] F. Franchini, A. Its, V. Korepin, and L. Takhtajan, Quant.Inf.Proc. **10**, 325 (2011).
[5] V. Alba, M. Haque, and A. M. Läuchli, J. Stat. Mech. Theor. Exp. **8**, 11 (2012).
[6] V. Alba, M. Haque, and A. M. Läuchli, Phys. Rev. Lett. **108**, 227201 (2012).
[7] P. Calabrese and A. Lefevre, Phys. Rev. A **78**, 032329 (2008).
[8] F. Pollmann, A. M. Turner, E. Berg, and M. Oshikawa, Phys. Rev. B **81**, 064439 (2010).
[9] F. Pollmann and J. E. Moore, New Journal of Physics **12**, 025006 (2010).
[10] A. M. Läuchli, ArXiv e-prints (2013), arXiv:1303.0741 [cond-mat.stat-mech].
[11] S. Giampaolo, S. Montangero, F. Dell'Anno, S. De Siena, and F. Illuminati, Phys. Rev. B **88**, 125142 (2013).
[12] T. Morimoto, H. Ueda, T. Momoi, and A. Furusaki, Phys. Rev. B **90**, 235111 (2014).
[13] G. Torlai, L. Tagliacozzo, and G. D. Chiara, J. Stat. Mech. Theor. Exp. **2014**, P06001 (2014).
[14] J. Mlter, T. Barthel, U. Schollwck, and V. Alba, J. Stat. Mech. Theor. Exp. **2014**, P10029 (2014).
[15] D. Poilblanc, Phys. Rev. Lett. **105**, 077202 (2010).
[16] I. Peschel and M.-C. Chung, EPL (Europhysics Letters) **96**, 50006 (2011).
[17] A. M. Läuchli and J. Schliemann, Phys. Rev. B **85**, 054403 (2012).
[18] J. Schliemann and A. M. Läuchli, J. Stat. Mech. Theor. Exp. **11**, 21 (2012).
[19] S. Tanaka, R. Tamura, and H. Katsura, Phys. Rev. A **86**, 032326 (2012).
[20] R. Lundgren, V. Chua, and G. A. Fiete, Phys. Rev. B **86**, 224422 (2012).
[21] R. Lundgren, Y. Fuji, S. Furukawa, and M. Oshikawa, Phys. Rev. B **88**, 245137 (2013); Phys. Rev. B **92**, 039903 (2015).
[22] X. Chen and E. Fradkin, J. Stat. Mech. Theor. Exp. **2013**, P08013 (2013).
[23] O. S. Zozulya, M. Haque, K. Schoutens, and E. H. Rezayi, Phys. Rev. B **76**, 125310 (2007).
[24] M. Haque, O. Zozulya, and K. Schoutens, Phys. Rev. Lett. **98**, 060401 (2007).
[25] A. M. Läuchli, E. J. Bergholtz, and M. Haque, New J. Phys. **12**, 075004 (2010).
[26] R. Thomale, A. Sterdyniak, N. Regnault, and B. A. Bernevig, Phys. Rev. Lett. **104**, 180502 (2010).
[27] A. M. Läuchli, E. J. Bergholtz, J. Suorsa, and M. Haque, Phys. Rev. Lett. **104**, 156404 (2010).
[28] Z. Liu, E. J. Bergholtz, H. Fan, and A. M. Läuchli, Phys. Rev. B **85**, 045119 (2012).
[29] A. Sterdyniak, A. Chandran, N. Regnault, B. A. Bernevig, and P. Bonderson, Phys. Rev. B **85**, 125308 (2012).
[30] J. Dubail, N. Read, and E. H. Rezayi, Phys. Rev. B **85**, 115321 (2012).
[31] I. D. Rodriguez, S. H. Simon, and J. K. Slingerland, Phys. Rev. Lett. **108**, 256806 (2012).
[32] I. D. Rodriguez, S. C. Davenport, S. H. Simon, and J. K. Slingerland, Phys. Rev. B **88**, 155307 (2013).
[33] A. Chandran, M. Hermanns, N. Regnault, and B. A. Bernevig, Phys. Rev. B **84**, 205136 (2011).
[34] N. Regnault and B. A. Bernevig, Phys. Rev. X **1**, 021014 (2011).
[35] M. Hermanns, Y. Salimi, M. Haque, and L. Fritz, J. Stat. Mech. Theor. Exp. **2014**, P10030 (2014).
[36] V. Alba, M. Haque, and A. M. Läuchli, Physical Review Letters **110**, 260403 (2013).
[37] F. Kolley, S. Depenbrock, I. McCulloch, U. Schollwöck, and V. Alba, Phys. Rev. B **88**, 144426 (2013).
[38] A. M. Turner, Y. Zhang, and A. Vishwanath, Phys. Rev. B **82**, 241102 (2010).
[39] L. Fidkowski, Phys. Rev. Lett. **104**, 130502 (2010).
[40] A. Alexandradinata, T. L. Hughes, and B. A. Bernevig, Phys. Rev. B **84**, 195103 (2011).
[41] M. Kargarian and G. A. Fiete, Phys. Rev. B **82**, 085106 (2010).
[42] C. Fang, M. J. Gilbert, and B. A. Bernevig, Phys. Rev. B **87**, 035119 (2013).
[43] X. Deng and L. Santos, Phys. Rev. B **84**, 085138 (2011).
[44] A. M. Turner, F. Pollmann, and E. Berg, Phys. Rev. B **83**, 075102 (2011).
[45] A. Hamma, R. Ionicioiu, and P. Zanardi, Phys. Rev. A **71**, 022315 (2005).
[46] S. Furukawa and G. Misguich, Phys. Rev. B **75**, 214407 (2007).
[47] H. Yao and X.-L. Qi, Phys. Rev. Lett. **105**, 080501 (2010).
[48] R. A. Santos, Phys. Rev. B **87**, 035141 (2013).
[49] J. Dubail and N. Read, Phys. Rev. Lett. **107**, 157001 (2011).
[50] J. Schliemann, New Journal of Physics **15**, 053017 (2013).
[51] J. Schliemann, J. Stat. Mech. Theor. Exp. **2014**, P09011 (2014).
[52] K. Shinjo, S. Sota, and T. Tohyama, ArXiv e-prints (2014), arXiv:1410.4790 [cond-mat.str-el].
[53] W. W. Ho, L. Cincio, H. Moradi, D. Gaiotto, and G. Vidal, ArXiv e-prints (2014), arXiv:1411.6932 [cond-mat.str-el].
[54] T. Giamarchi, *Quantum Physics in One Dimension* (Oxford University Press, New York, 2013).
[55] A. O. Gogolin, A. A. Nersesyan, and A. M. Tsvelik, *Bosonization and Strongly Correlated Systems* (Cambridge University Press, New York, 1998).
[56] R. Thomale, D. P. Arovas, and B. A. Bernevig, Phys. Rev. Lett. **105**, 116805 (2010).
[57] R. Lundgren, J. Blair, M. Greiter, A. Läuchli, G. A. Fiete, and R. Thomale, Phys. Rev. Lett. **113**, 256404 (2014).
[58] I. Mondragon-Shem, M. Khan, and T. Hughes, Phys. Rev. Lett. **110**, 046806 (2013).
[59] E. C. Andrade, M. Steudtner, and M. Vojta, J. Stat. Mech. Theor. Exp. **2014**, P07022 (2014).
[60] R. Lundgren, J. Blair, P. Laurell, N. Regnault, G. A. Fiete, M. Greiter, and R. Thomale, ArXiv e-prints (2015), arXiv:1512.09030 [cond-mat.str-el].

[61] L. A. Pando Zayas and N. Quiroz, ArXiv e-prints (2014), arXiv:1407.7057 [hep-th].
[62] V. Balasubramanian, M. McDermott, and M. Van Raamsdonk, Phys. Rev. D **86**, 045014 (2012).
[63] R. A. Santos, ArXiv e-prints (2014), arXiv:1408.1716 [cond-mat.str-el].
[64] R. A. Santos, C.-M. Jian, and R. Lundgren, ArXiv e-prints (2015), arXiv:1511.01489 [cond-mat.str-el].
[65] J. Eisert, M. Cramer, and M. Plenio, Rev. Mod. Phys. **82**, 277 (2010).
[66] G. Gori, S. Paganelli, A. Sharma, P. Sodano, and A. Trombettoni, Phys. Rev. B **91**, 245138 (2015).
[67] N. Shiba and T. Takayanagi, Journal of High Energy Physics **2014**, 33 (2014), 10.1007/JHEP02(2014)033.
[68] G. Vitagliano, A. Riera, and J. I. Latorre, New Journal of Physics **12**, 113049 (2010).
[69] G. Ramrez, J. Rodrguez-Laguna, and G. Sierra, Journal of Statistical Mechanics: Theory and Experiment **2014**, P10004 (2014).
[70] S. Furukawa and Y. Kim, Phys. Rev. B **83**, 085112 (2011).
[71] A. Mollabashi, N. Shiba, and T. Takayanagi, J. High Energy Phys. **2014**, 185 (2014), 10.1007/JHEP04(2014)185.
[72] J. C. Xavier and F. B. Ramos, Journal of Statistical Mechanics: Theory and Experiment **2014**, P10034 (2014).
[73] E. Kim and J. Sólyom, Phys. Rev. B **60**, 15230 (1999).
[74] S. Furukawa, M. Sato, S. Onoda, and A. Furusaki, Phys. Rev. B **86**, 094417 (2012).
[75] F. D. M. Haldane, Phys. Rev. Lett. **47**, 1840 (1981).
[76] J. Cano, T. L. Hughes, and M. Mulligan, ArXiv e-prints (2014), arXiv:1411.5369 [cond-mat.str-el].
[77] I. Peschel, J. Physics A: Mathematical and General **36**, L205 (2003).
[78] There are other possible paths, which can be used to control phase factors [85], However, the left and right moving particles are not free when the legs of ladder are uncoupled and at the XX point.
[79] F. m. c. Crépin, N. Laflorencie, G. Roux, and P. Simon, Phys. Rev. B **84**, 054517 (2011).
[80] C.-M. Chung, L. Bonnes, P. Chen, and A. M. Läuchli, Phys. Rev. B **89**, 195147 (2014).
[81] D. J. Luitz, X. Plat, N. Laflorencie, and F. Alet, Phys. Rev. B **90**, 125105 (2014).
[82] N. M. Tubman and D. C. Yang, Phys. Rev. B **90**, 081116 (2014).
[83] N. M. Tubman and D. ChangMo Yang, ArXiv e-prints (2014), arXiv:1412.1495 [cond-mat.str-el].
[84] A. Nersesyan, A. Gogolin, and F. Eßler, Phys. Rev. Lett. **81**, 910 (1998).
[85] X. Dai and Z.-b. Su, Phys. Rev. B **57**, 964 (1998).